Steady Marangoni flow traveling with chemical fronts

L. Rongy[a)] and A. De Wit[b)]
Service de Chimie Physique et Biologie Théorique and Center for Nonlinear Phenomena and Complex Systems, CP 231, Université Libre de Bruxelles, 1050 Brussels, Belgium

When autocatalytic chemical fronts propagate in thin layers of solution in contact with air, they can induce capillary flows due to surface tension gradients across the front (Marangoni flows). We investigate here such an interplay between autocatalytic reactions, diffusion, and Marangoni effects with a theoretical model coupling the incompressible Navier-Stokes equations to a conservation equation for the autocatalytic product concentration in the absence of gravity and for isothermal conditions. The boundary condition at the open liquid/air interface takes the surface activity of this product into account and introduces the solutal Marangoni number M representing the intensity of the coupling between hydrodynamics and reaction-diffusion processes. Positive and negative Marangoni numbers correspond, respectively, to the cases where the product decreases or increases surface tension behind the front. We show that, in both cases, such coupled systems reach an asymptotic dynamics characterized by a steady fluid vortex traveling at a constant speed with the front and deforming it, with, however, an asymmetry between the results for positive and negative M. A parametric study shows that increased propagation speed, front deformation, and possible transient oscillating dynamics occur when the absolute value of M is increased. © *2006 American Institute of Physics*. [DOI: 10.1063/1.2186313]

I. INTRODUCTION

Chemical fronts propagating at constant speed are well-known examples of pattern formation resulting from the coupling of diffusion and nonlinear reaction kinetics such as autocatalysis.[1–3] Their properties, studied experimentally in gels to avoid any convection, are nowadays well characterized.[4] However, studies of the propagating velocities of these waves in aqueous solutions have sometimes revealed behaviors that cannot be explained solely by reaction-diffusion processes.

For example, wave fronts of the iodate-arsenous acid reaction have long been noted to propagate with velocities increasing with time in a thin layer of solution in contact with air when iodate is in excess.[5,6] Similarly, Bazsa and Epstein have performed experimental studies of the velocity of front propagation in the nitric acid-iron(II) reaction in Petri dishes open to the air.[7] They noted that the velocity of the waves depends on the depth of the solution layers and that these two-dimensional (2D) waves do not travel at a constant velocity but accelerate. Increasing the viscosity of the solvent with either fine glass powder or with silica gel results in constant propagation speed, independent of the geometric parameters of the setup. Therefore it was suggested that convection resulting from a combination of Marangoni and buoyancy effects may play an important role in such systems.[8]

The role of hydrodynamics in the evolution of chemical systems driven far from equilibrium has long been emphasized in the case of spatial structures generated at diverse interfaces.[9–13] In the case of chemical front systems, the spatiotemporal distribution of heat and mass resulting from the front propagation can affect the density, the viscosity, and the surface tension of the reaction solution, thereby eventually initiating convection.

Experimentally, convection was shown to influence transient precipitation patterns of $BaSO_4$ behind the traveling wave in the chlorite-thiourea-barium chloride reaction system. The origin of these patterns is qualitatively discussed in terms of coupling between thermocapillary (surface tension-driven) and multicomponent (buoyancy-driven) convections, via the formation of convective tori at the wave front.[14–16] Other studies on hydrodynamic flow associated with chemical wave propagation are reported both in covered and uncovered thin layers of the Belousov-Zhabotinskii (BZ) solution. Some papers report on oscillatory flow induced by spiral waves and subsequent periodic deformation of these waves,[17–19] sometimes leading to their turbulent decomposition,[20] and to propagation of surface deformation.[21] An accelerating chemical wave, also called *big wave*, accompanied by large hydrodynamic motions and surface deformation propagation has also been experimentally well characterized.[22–26] Transduction of these chemically driven flows into spontaneous motion of an aqueous droplet of BZ reaction medium on an oil phase has even been evidenced.[27,28] Since the BZ reaction is an exothermic reaction involving surface-active compounds,[29,30] inhomogeneities in surface tension or in density are supposed to play a key role in these fluid motions even though detailed understanding of the underlying mechanisms and of their parametric dependence is still lacking.

The complexity of such experimental systems arises from the fact that it is not always trivial to discriminate be-

---

a)Electronic mail: lrongy@ulb.ac.be
b)Electronic mail: adewit@ulb.ac.be

tween surface-tension-driven and buoyancy-driven convections. In addition, as the kinetics, the composition across the front, and the heat released due to the exothermicity of the reaction all depend on the initial concentrations of reactants, it is clear that the relative importance of Marangoni and buoyancy flows can vary in the parameter space for a same reaction. In this framework, theoretical approaches are crucial to discriminate the influence of the various effects thanks to the analysis of model systems where only one type of convective flow is active.

Theoretical studies of pure buoyancy-driven flows around chemical waves propagating horizontally have shown that these flows lead to a deformation and acceleration of the front.[31–36] Numerical comparison between Marangoni and buoyancy-driven flows around BZ chemical waves have been performed by Matthiessen *et al.* by numerically solving modified Oregonator model equations coupled to the Navier-Stokes equations.[37] By the same type of approach, Diewald *et al.* enlightened the capillary origin of oscillating flows observed at the passage of BZ waves[38] while Kitahata *et al.* discussed the periodic motion of a BZ droplet floating on an oil phase.[27] The dynamics resulting from the coupling between pure Marangoni effects and bulk insoluble reactants involved in an autocatalytic reaction occurring solely at the surface has been modeled using lubrication theory by Dagan and Pismen[39] as well as Dagan and Maldarelli.[40] Bistable surface chemical reactions involving a single reactant supplied from the bulk have also been considered theoretically by Pismen in connection with Marangoni flows.[41] In the same spirit, coupling a bistable chemical reaction taking place at the interface of a deep fluid and involving an insoluble surfactant to diffusion and Stokes equations, Pismen pointed out the existence of interfacial solitary structures generated by the reaction and stabilized by Marangoni flow.[42] Such interesting approaches are, however, linked to reactions occurring only at the surface and fail therefore to describe the deformations of chemical fronts in the bulk where reactions also take place.

In this framework, it is the objective of this article to study numerically the spatiotemporal dynamics of a model chemical front subjected to solutal capillary forces in the absence of gravity. Our goal is to characterize quantitatively the acceleration and deformation of a front traveling in the bulk of a reactive solution layer open to the air and subjected to Marangoni flows driven by concentration variations across the front. As the various chemo-hydrodynamic regimes observed experimentally around propagating chemical waves can be quite involved, we intentionally study here the simplest possible model in order to understand what type of dynamics can be expected from pure Marangoni effects in the absence of gravity. In this regard, we focus on traveling chemical fronts resulting from a one-variable cubic kinetics coupled to diffusion. This allows to avoid complex flows around pulses or wave trains and the necessity of considering more than one chemical species. In the same spirit, we consider that capillary flows are induced solely by concentration gradients across the front, i.e., that thermal effects are negligible here so that the reaction is treated as isothermal. This approach allows us to characterize in detail chemically
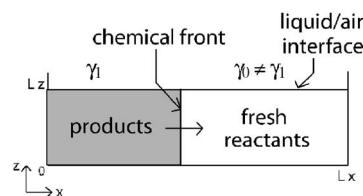

FIG. 1. Sketch of the system.

driven Marangoni flows and their dependence on the intensity of the coupling parameter which is the Marangoni number. We show that, after a given transient, the reaction-diffusion (RD)-convection system evolves towards an asymptotic regime in which a steady vortex driven by the soluto-capillary forces travels with the chemical front and deforms it. Comparison of the dynamics for, respectively, positive and negative Marangoni numbers is proposed.

The article is organized as follows. In Sec. II, we introduce a simple model for an autocatalytic reaction producing a surface-active species and capable of generating propagating fronts that we couple to molecular diffusion and Marangoni convection. The influence of concentration gradients on surface-tension-induced capillary flows is related to the boundary condition at the open liquid/air interface, introducing the solutal Marangoni number M increasing with the intensity of the coupling. In Sec. III, we analyze the characteristics of the capillary-induced flow and the nonlinear dynamics of the reaction-diffusion-convection front as a function of M. We observe the reach of an asymptotic dynamics characterized by a constant propagation speed of a chemical front deformed by an asymmetric convection roll. We compare the properties of this asymptotic solitary reactive vortex when the product decreases ($M>0$) or increases ($M<0$) the surface tension behind the front, showing an asymmetry in the results. Conclusions are drawn in Sec. IV.

II. MODEL AND NUMERICAL METHOD

A. Equations of motion

We consider a 2D thin aqueous solution layer of length L_x and height L_z, corresponding to a vertical cut in a Petri dish (see Fig. 1). An isothermal planar chemical front producing a surface-active species propagates along the x direction with the surface tension of the products γ_1 different from that of the reactants γ_0. We assume no surface deformation and no evaporation, so that the air layer is not considered here. We furthermore neglect the possible density variations due to the chemical reaction and we regard the solution density as constant in space and time. As a model system, we consider the autocatalytic reaction

$$A + 2C \rightarrow 3C. \tag{1}$$

The kinetics of this reaction is given by $f(c)=kac^2$ where k is the rate constant for the reaction and a and c are the chemical concentrations. This kinetics is capable of sustaining traveling fronts between two different states when coupled to molecular diffusion and describes chemical systems such as the iodate-arsenous acid redox reaction.[1,6,43] We can reduce this autocatalytic kinetics to the simple one-variable cubic ex-

pression $f(c)=kc^2(a_0-c)$, where a_0 is the initial reactant concentration, thanks to the stoichiometric relation locally valid between a and c if we assume the diffusion coefficients of both species to be equal. The only chemical variable is then the concentration c of the autocatalytic product that we assume to be surface active. The transport phenomena acting on this species are molecular diffusion and convection of the fluid. Hence, the governing equations for this system are obtained by coupling the reaction-diffusion-advection equation for the surface-active substance to the incompressible Navier-Stokes equations, namely,

$$\frac{\partial c}{\partial t} + \underline{v}.\nabla c = D\nabla^2 c + f(c), \tag{2}$$

$$\frac{\partial \underline{v}}{\partial t} + \underline{v}.\nabla \underline{v} = \nu\nabla^2 \underline{v} - \frac{1}{\rho_0}\nabla p + \underline{g}, \tag{3}$$

$$\text{div } \underline{v} = 0, \tag{4}$$

where $\underline{v}=(u,w)$ is the 2D fluid velocity vector, p denotes the pressure, and $\underline{g}=(0,-g)$ is the gravity acceleration. The solution density ρ_0, the kinematic viscosity $\nu=\mu/\rho_0$, where μ is the dynamic viscosity, and the molecular diffusion coefficient D are assumed to be constant.

Our rectangular system has rigid side walls, a rigid bottom, and a free upper surface. At each boundary of this domain we require zero-flux boundary conditions for the chemical concentration c. The hydrodynamic boundary conditions at the rigid boundaries are no-slip conditions, $u=0$ and $w=0$. At the free surface we require $w=0$ and we use a Marangoni boundary condition for the horizontal fluid velocity u to include the changes in surface tension induced by the concentration gradient of the surface-active product across the front:[44]

$$\mu\frac{\partial u}{\partial z} = \frac{\partial \gamma}{\partial x} \quad \text{at } z=L_z, \tag{5}$$

where γ is the surface tension of the solution.

To nondimensionalize the problem, we introduce the dimensionless variables $c'=c/a_0$, $t'=t/\tau_c$, $x'=x/L_c$, $z'=z/L_c$, $\underline{v}'=\underline{v}/U_c$, and $p'=p/p_c$ where we use the characteristic scales of the reaction-diffusion system: for time, $\tau_c=1/ka_0^2$, for length, $L_c=\sqrt{D\tau_c}$, and for velocity, $U_c=L_c/\tau_c=\sqrt{D/\tau_c}$. Here $p_c=\rho_0 S_c D/\tau_c$ where the dimensionless parameter $S_c=\nu/D$ is the Schmidt number. We define in addition a new hydrostatic pressure gradient incorporating the constant buoyancy term as $\nabla'p''=\nabla'p'-\rho_0 L_c\underline{g}/p_c$.

Dropping all the primes and incorporating a linear dependence between the surface tension and the surfactant concentration, $\gamma=\gamma_0+(d\gamma/dc)c$ with γ_0 the surface tension of pure water, we obtain the dimensionless evolution equations

$$\frac{\partial c}{\partial t} + \underline{v}.\nabla c = \nabla^2 c + c^2(1-c), \tag{6}$$

$$\frac{\partial \underline{v}}{\partial t} + \underline{v}.\nabla \underline{v} = S_c \cdot (-\nabla p + \nabla^2 \underline{v}), \tag{7}$$

$$\text{div } \underline{v} = 0, \tag{8}$$

with the following boundary conditions:

$$\frac{\partial c}{\partial x} = 0 = u = w, \quad x=0, \quad x=L_x, \tag{9}$$

$$\frac{\partial c}{\partial z} = 0 = u = w, \quad z=0, \tag{10}$$

$$\frac{\partial c}{\partial z} = 0 = w, \quad z=L_z, \tag{11}$$

$$\frac{\partial u}{\partial z} = -M\frac{\partial c}{\partial x}, \quad z=L_z \tag{12}$$

where L_x and L_z now represent, respectively, the dimensionless length and height of the layer. Condition (12) is the dimensionless form of Eq. (5) and introduces the dimensionless solutal Marangoni number M:

$$M = \frac{-1}{\mu\sqrt{Dk}}\frac{d\gamma}{dc}. \tag{13}$$

Notice that the Marangoni number is positive (negative) if the surface-active product decreases (increases) the surface tension behind the front. Marangoni numbers are usually defined in the literature using hydrodynamic characteristic scales but here we have used the characteristic scales of the reaction-diffusion system so that we obtain a chemical Marangoni number inversely proportional to the square root of the kinetic constant k of the chemical reaction. This number quantifies the coupling strength between the hydrodynamic motions and the RD processes and is therefore the key parameter of our model.

The initial condition corresponds to a planar reaction-diffusion front propagating in a solution in the absence of any fluid flow. Hence, the initial fluid velocity and the hydrostatic pressure gradient are zero everywhere in the system. The initial condition for the surface-active product concentration is the convectionless RD profile.

In Sec. III we perform the numerical integration of the dimensionless model [(6)–(12)] in order to characterize the hydrodynamic motion initiated by the Marangoni effects and its influence on the RD front dynamics. In this framework, let us first recall the properties of such a front in the absence of flow.

B. Reaction-diffusion front

In the absence of flow, i.e., for a Marangoni number equal to zero, Eq. (6)–(8) with $\underline{v}=0$ reduce to

$$\frac{\partial c}{\partial t} = \nabla^2 c + c^2(1-c). \tag{14}$$

The $c=1$ solution is the kinetically stable chemical steady state corresponding to the reaction products invading the $c=0$ solution corresponding to the marginally stable fresh reactants. Equation (14) allows exact analytical integration and admits as solution the following propagating front:[1,6,43]

$$c(x,t) = \frac{1}{1 + e^{(x-vt)/\sqrt{2}}} = \frac{1}{2}\left[1 + \tanh\left(-\frac{\sqrt{2}}{4}(x-vt)\right)\right],$$

$$(15)$$

where v is the constant RD speed of the front, equal to

$$v = \sqrt{2}/2. \qquad (16)$$

The width w_{RD} of this front, arbitrarily defined as the distance between $c=0.99$ and $c=0.01$, equals

$$w_{RD} = 2\sqrt{2}\ln 99 = 13. \qquad (17)$$

This planar chemical front results from the coupling between diffusion and autocatalytic reaction (1) and corresponds to the products ($c=1$) invading the reactants ($c=0$) with a constant speed v and a constant width w_{RD}. Let us note that other definitions of the width of the front could have been used.[45] Our definition has the advantage of allowing for an easy study of the deformation of the front by Marangoni flows in the depth of the layer by a simple tracking of the $c=0.01$ and $c=0.99$ isoconcentration lines as will be shown in Sec. III.

C. Numerical method and validation studies

To analyze the nonlinear dynamics of a chemical front propagating in the presence of a Marangoni effect, we integrate the governing equations of our reaction-diffusion-convection model numerically. Equations (6)–(8) are solved in primitive variables by a finite-difference method. The domain is discretized using a uniform rectangular mesh. Forward differences in time and second-order central differences in space are used to discretize the partial differential equations. Our numerical code uses a semi-implicit projection method in which only the pressure gradient term in Eq. (7) and the continuity equation (8) are treated implicitly. At each time step, the new product concentration c is calculated and the computation of the velocity field is split into two substeps. In the first one, a provisional nonsolenoidal velocity field is calculated neglecting the pressure gradient term in Eq. (7). In the second substep, the pressure field is calculated from a Poisson equation by means of a successive over-relaxation (SOR) iterative method[46] with the boundary conditions prescribed by Gresho and Sani.[47] The accuracy of the solution for the pressure is fixed to 10^{-6}. The provisional velocity field is next projected onto the space of divergence-free velocity fields using the computed pressure field.

Our numerical code has been validated through comparison with known analytical results. When the Marangoni number M is equal to zero, we numerically recover the planar traveling front (15) with the correct speed (16) and width (17). To check the accuracy of the integration of the incompressible Navier-Stokes equations we tested that we reproduce the analytical results for the return flow that develops in an infinite thin layer of solution when the temperature of the free surface is fixed at $T=x$, where x is the horizontal coordinate.[44]

The solutions of Eqs. (6)–(8) were found to converge on decreasing the temporal and spatial step sizes. Our integration mesh is rectangular because a higher precision is necessary in the z direction along the thin layer thickness than in the front propagation direction x. Indeed, the convective motions are initiated through boundary condition (12) involving an important gradient along z, whereas the gradients along x are less sharp. Typically the spatial step sizes are $dx=0.5$ and $dz=0.25$. The corresponding time step is $dt=5.10^{-6}$.

III. CHEMICALLY INDUCED MARANGONI CONVECTION AND INFLUENCE ON THE FRONT PROPAGATION: NONLINEAR DYNAMICS

In this section, we present the results of the numerical integration of Eqs. (6)–(8) subjected to the boundary and initial conditions described in Sec. II A. Our model includes four dimensionless parameters: two hydrodynamic parameters, the Marangoni number M and the Schmidt number S_c, and two parameters related to the domain geometry, L_x and L_z. The Marangoni number here is a measure of the interaction strength between the reaction-diffusion processes and the hydrodynamic flow, and will therefore be progressively increased to consider an increasingly important coupling. We compute a typical Schmidt number, $S_c = \mu/\rho_0 D$, from the viscosity and the density values of water. To work with realistic values of the diffusion coefficient D of species involved in autocatalytic reactions,[2,43] we use D in the range $(0.7-2) \times 10^{-5}$ cm^2/s. This gives a range of Schmidt numbers varying between 500 and 1500. The numerical results are quantitatively the same whatever value we choose between those limits, which means that we effectively analyze a Stokes flow. The length of the system, L_x, as well does not influence the numerical results provided that the system is long enough for the lateral boundaries not to affect the dynamics. The value of the dimensionless layer thickness, L_z, is taken as in the same order of magnitude as the dimensionless width of the RD front ($w_{RD}=13$) because we consider a quite thin layer up to 1 mm in thickness, which is more or less the order of magnitude of the width of a chemical front.[6] Therefore, L_z was chosen to be equal to 10.

Let us now consider the spatiotemporal evolution of this system. When $M=0$, no hydrodynamic motion appears in the solution and the planar front propagates without any deformation at the constant RD propagation speed v. When the Marangoni number differs from zero, we need to consider two different situations according to the sign of M.

A. Positive Marangoni numbers

Let us first consider the case of positive Marangoni numbers for which the product decreases the surface tension behind the front. We can then observe the onset of a surface-tension-driven flow due to the concentration gradient of the surface-active product across the front. At the surface the flow is initiated towards the region with larger surface tension, here the reactants, i.e., in the same direction as the RD speed. This surface flow towards the right induces a bulk flow in the opposite direction since we consider an incompressible flow in a closed system. The influence on the chemical front propagation of such Marangoni-driven convection is shown in Fig. 2 for a Marangoni number equal to
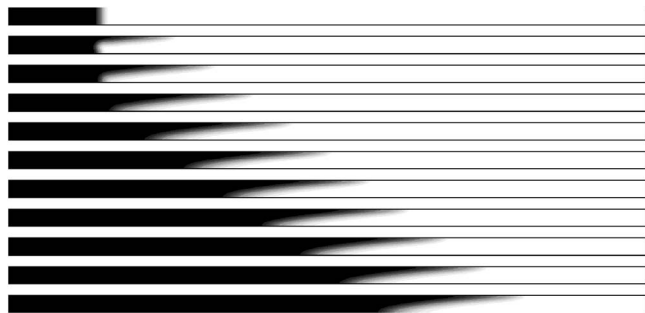
FIG. 2. Propagation of a chemical front in the presence of chemically induced Marangoni convection for $M=100$ shown from top to bottom from $t=0$ up to $t=50$ with a time interval of $\Delta t=5$. The aspect ratio between $L_x=350$ and $L_z=10$ is preserved.

100. The dynamics is represented by two-dimensional density plots of the product concentration ranging from $c=0$ (white) to $c=1$ (black) for increasing time.

First the front is accelerated at the surface because of the capillary flow induced by the surface tension gradient. This surface acceleration is followed by initiation of a return flow in the bulk. A convection roll develops in the layer and induces a visible distortion of the front into the depth. The width of the deformation zone increases on the short times but, quite rapidly, a solitary structure consisting in a flow vortex surrounding the propagating front reaches an asymptotic constant speed and steady shape. Typically, after 25 τ_c, a stationary regime is reached in which the front propagates at a constant speed V six times larger than the RD speed v without convection. The front distortion and the fluid velocity field remain invariant in the comoving frame. Our numerical results indicate that the asymptotic velocity field traveling with the front is an asymmetric convection roll localized in the region of the front. As v is zero everywhere else in the system, the focus of Fig. 3 is put only on the region of the deformed front. This convection roll is asymmetric along both directions with a pronounced downward flow of short spatial extent at the tip and a weaker upward flow distributed over a broader zone at the back. As seen in Fig. 3, the convection roll is not exactly centered on the front but slightly shifted forward and localized at the tip of the front.

Due to the convective motions, the translation symmetry along the z direction has been broken and the concentration profiles taken at different heights are more stretched than those without convection. The asymptotic width w_{RDC} of the
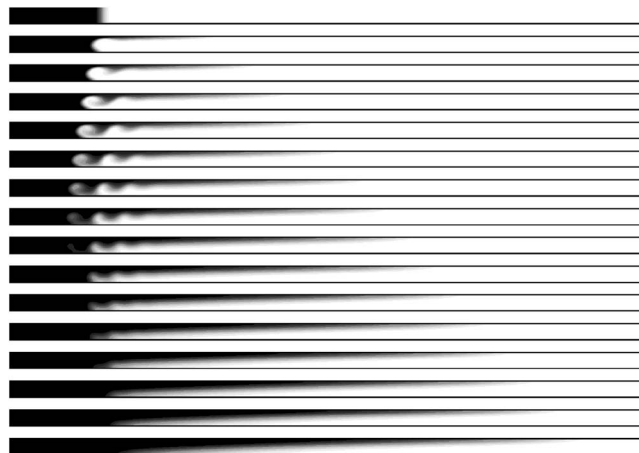

FIG. 4. Transient oscillating deformation of a chemical front due to chemically induced Marangoni convection at high Marangoni number ($M=1000$). The dynamics is shown from top to bottom from $t=0$ up to $t=15$ with a time interval of $\Delta t=1$. The aspect ratio between $L_x=350$ and $L_z=10$ is preserved.

transition zone between the products (at $c>0.99$) and the reactants (here with $c<0.01$) is now a function of z and is larger than the RD front width w_{RD} [Eq. (17)]. Our results show that $w_{\mathrm{RDC}}(z)$ is maximum around $z=6.5$ for all the positive Marangoni numbers we have studied. For $M=100$, the maximum width is equal to 80.0 ± 0.5, namely, more than six times the reaction-diffusion front width w_{RD} given by (17), this effect increasing with M.

For values of the Marangoni number typically larger than $M=220$, several convection rolls initially appear leading to a wavy-concentration profile (Fig. 4). The number of vortices increases at the beginning but they disappear after a short time as the transient velocity field evolves towards one final convection roll traveling with the asymptotic front. The larger M, the more pronounced the oscillations of concentration and fluid velocity, but for each value of the Marangoni number we have screened (i.e., $0 \leq M \leq 1000$) the system reaches an asymptotic dynamics after roughly the same time (around 25 τ_c). Therefore it is interesting to characterize this asymptotic dynamics as a function of M by comparing the deformation of the front, its constant propagation speed, and the asymptotic convection roll traveling with this front.

To do so, the steady 2D concentration field $c(x-V(M)t,z)$ traveling at the constant propagation speed $V(M)$ can be spatially averaged along the z coordinate to yield the one-dimensional averaged profile
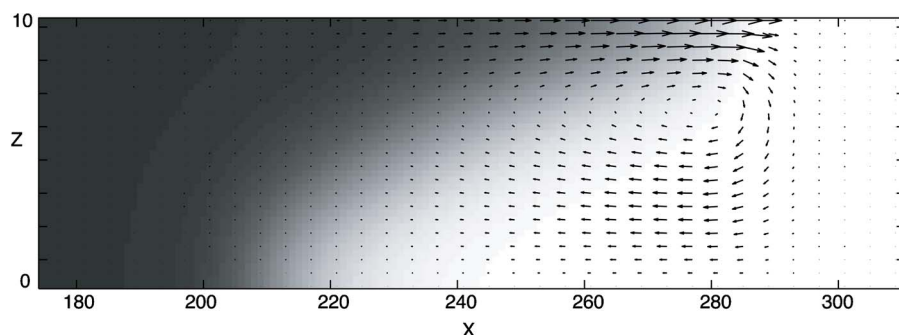

FIG. 3. Focus on the asymptotic asymmetric convection roll traveling with the deformed front for $M=100$. Due to the thinness of the layer, the aspect ratio of such plots is not respected here but the z direction has been magnified in order to see the details of the velocity field.
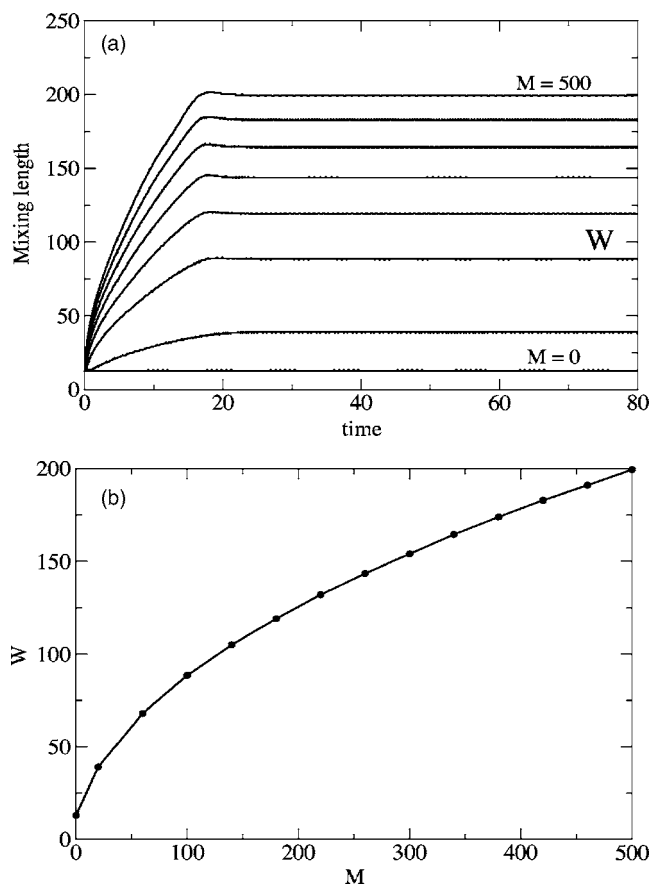
FIG. 5. (a) Mixing lengths as a function of time for various positive Marangoni numbers, $M=0$, 20, 100, 180, 260, 340, 420, and 500 from bottom to top and (b) asymptotic mixing length W as a function of the Marangoni number.

$$\langle c(x - V(M)t) \rangle = \frac{1}{L_z} \int_0^{L_z} c(x - V(M)t, z) dz.$$

This averaged profile can then be used to define the tip and rear of the deformed front. The tip is chosen arbitrarily as the position along x in front of which the averaged concentration is less than 0.01, and the rear corresponds on the other hand to the position behind which the averaged concentration is larger than 0.99. The distance between the tip and the rear of the front can typically characterize the deformation of the front since it represents the extent of the transition zone between $\langle c \rangle = 1$ and $\langle c \rangle = 0$ which we will refer to as the mixing length. Figure 5(a) shows the mixing lengths computed as a function of time for various M. If $M=0$, the mixing length is constant and corresponds to the width w_{RD} of the RD front given by (17). For $M \neq 0$, the mixing lengths increase on the short times, representing the initial growth of the deformation zone. Next, there is saturation to a constant mixing length W characterizing the extent of the asymptotic deformation of the front. This saturation appears around the same time for the various Marangoni numbers, but the larger M, the more important the initial growth, and consequently, the larger W, as shown in Fig. 5(b).

Due to the presence of convective motions in the solution, the deformed front propagates at a constant speed $V > v$. This asymptotic speed V, determined as the slope of the
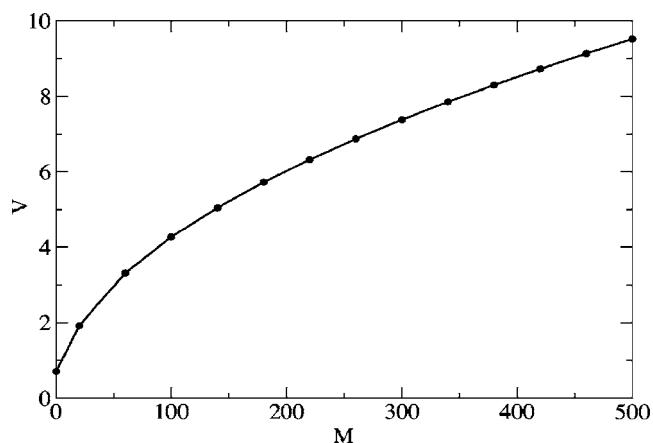
position of the tip as a function of time in the steady regime, is seen to increase nonlinearly with M (Fig. 6).

To characterize the convective motions, we plot the maximum absolute value of the asymptotic horizontal velocity u as a function of M (Fig. 7). The maximum value is always at the surface where $u > 0$ and is directed towards the reactants. We can notice that this maximum value is proportional to the square root of M. Another way to describe the asymptotic convection roll is to compare the velocity profiles taken at different heights for various M. However, the traveling speed of the roll, V, is a function of M, which makes a direct comparison difficult. Therefore, we arbitrarily define a new reference frame by shifting the position of $\langle c \rangle = 0.5$ to the same point $x' = 0$ for all Marangoni numbers. The velocity and concentration profiles can then be compared in the same reference frame $x - x_{\langle c \rangle = 0.5}$ for different M. It also allows us to check the reach of the asymptotic regime by superposing the concentration and velocity profiles at different times starting from $t = 25 \ \tau_c$.

Three types of asymptotic fluid velocity profiles (the horizontal velocity u at the surface and in the middle of the layer, and the vertical velocity w in the middle of the layer) are shown in Fig. 8 for different Marangoni numbers in the

FIG. 6. Asymptotic propagation speed V of the chemical front as a function of the Marangoni number.
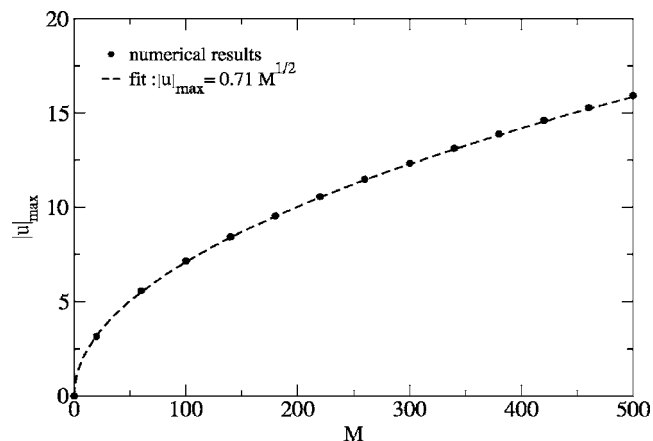
FIG. 7. Maximum absolute value of the asymptotic horizontal velocity u as a function of the Marangoni number. The broken line represents a square root fit of the numerical data.
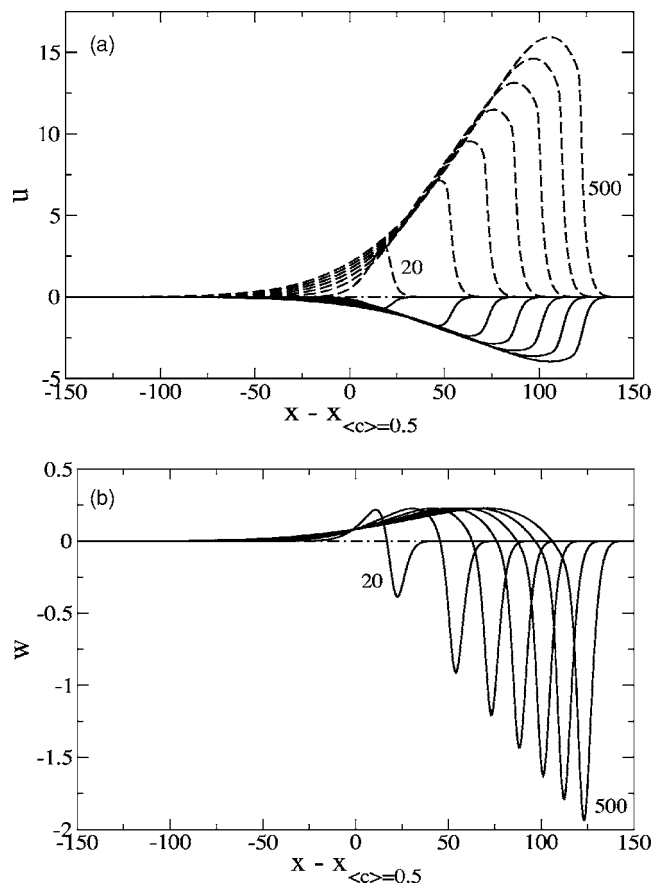
FIG. 8. Asymptotic profiles of (a) the horizontal velocity u at the surface (dashed lines) and in the middle of the layer (solid lines) and of (b) the vertical velocity w in the middle of the layer represented in the comoving frame for increasing positive Marangoni numbers between 20 and 500 with an interval of 80 between two successive curves. The dot-dashed curve corresponds to $M=0$ when there is no convection.

FIG. 9. Asymptotic profiles of (a) the averaged concentration $\langle c \rangle$ and of (b) the surface concentration represented in the comoving frame for increasing positive Marangoni numbers between 20 and 500 with an interval of 80 between two successive curves. The dot-dashed curve corresponds to the RD profile.

new comoving frame. These figures depict the asymmetry of the convection roll along both directions: the frontal parts of the profiles are stiffer than their back along x and the tangential velocity u is already negative at $z=L_z/2$, indicating that the position along z of zero velocity is shifted towards the surface. The asymmetry along x and the width of the convection roll increase with M, which can be correlated to the asymptotic averaged and surface concentration profiles, which are wider and more asymmetric at larger M (see Fig. 9). On the other hand, the vertical position of zero velocity is more or less independent of the Marangoni number we took, as can be seen in Fig. 10 representing the asymptotic profiles of the horizontal fluid velocity u across the layer. Those vertical cuts are performed at the position along x where $|u|$ is maximum for the various M and indicate that the flow changes its direction around $z=2L_z/3$ independently of the value of M. In the same way, the maximum and minimum values of u are located at the same heights of the layer, i.e., respectively, at the surface and at roughly $L_z/3$. On the contrary, the extrema of the u and v profiles along x are further away from the position of $\langle c \rangle = 0.5$ when M increases. This is due to the fact that the convective motions are generated at the surface following the gradient of the surface-active product concentration. The convection roll is then localized on the surface front whose distance from the averaged front in-
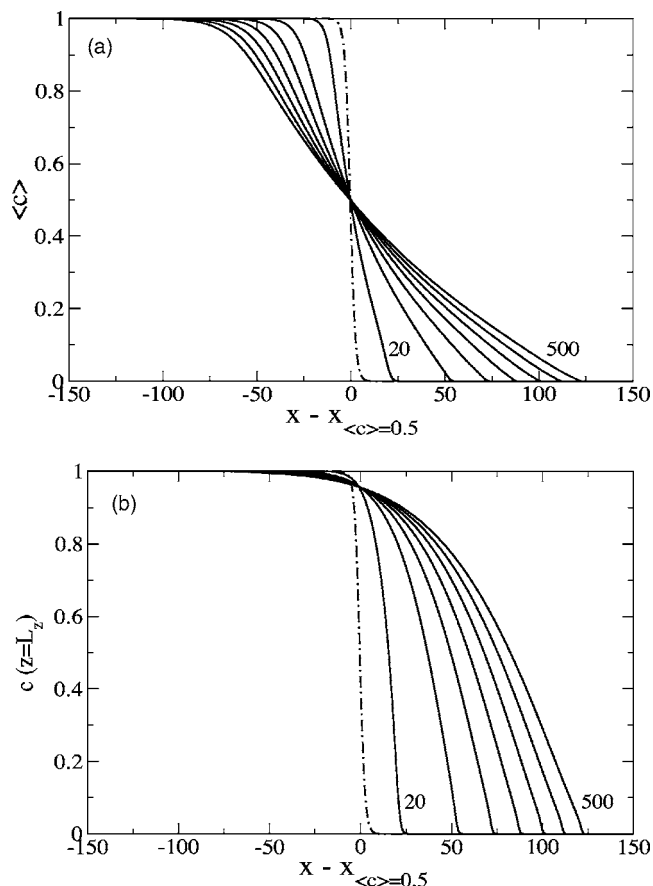
creases with M since the deformation of the planar front is more pronounced at large M. This can be observed in Fig. 9(b) where we see that the larger M, the further the surface concentration profile from $x=x_{\langle c \rangle = 0.5}$. A discussion of the properties of those profiles is given in Sec. III C.
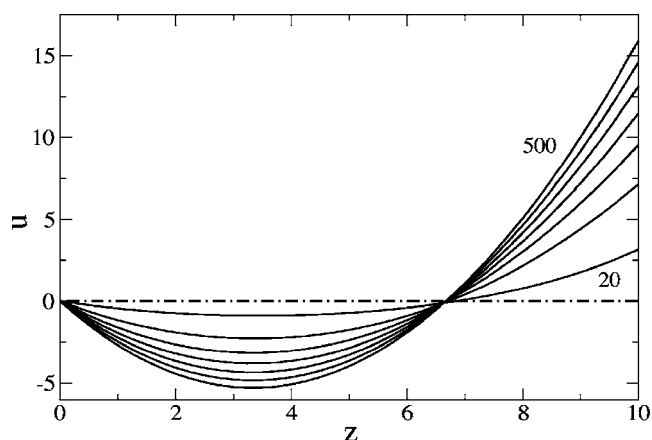

FIG. 10. Asymptotic profiles of the horizontal fluid velocity u across the layer at $x=x_{|u|=|u|_{max}}$ for increasing positive Marangoni numbers between 20 and 500 with an interval of 80 between two successive curves. The dot-dashed curve corresponds to $M=0$ when there is no convection.

FIG. 11. Propagation of a chemical front in the presence of chemically induced Marangoni convection for $M=-100$ shown from top to bottom from $t=0$ up to $t=50$ with a time interval of $\Delta t=5$. The aspect ratio between $L_x=350$ and $L_z=10$ is preserved.

FIG. 13. Propagation of a chemical front in the presence of chemically induced Marangoni convection with apparition of an additional deformation for $M=-1000$. The dynamics is shown from top to bottom from $t=0$ up to $t=50$ with a time interval of $\Delta t=5$. The aspect ratio between $L_x=350$ and $L_z=10$ is preserved.

B. Negative Marangoni numbers

Let us now consider the case of negative Marangoni numbers for which the product of the reaction increases the surface tension behind the front. Consequently, the flow is initiated at the surface towards the region of the products, in the direction opposite to that of the RD front propagation. In that case, the system also reaches an asymptotic dynamics, but earlier than for $M>0$. After usually roughly 10 τ_c, the front already propagates to the right at a constant speed and with an asymptotic shape (see, for example, Fig. 11 for $M=-100$). The deformation of the planar front is in the opposite direction compared with positive M. The asymptotic convection roll traveling with this front is also asymmetric in both directions but rotates now counterclockwise (Fig. 12).

As for $M>0$, the translation symmetry along the z direction is broken and hence, the steady width of the transition zone between the products and the reactants, w_{RDC}, is also a function of z. But, in this case, the effect of convection is different in the lower part of the layer where w_{RDC} is smaller than the RD width w_{RD}. In the upper part, $w_{RDC}>w_{RD}$ and increases with $|M|$. The position of maximum w_{RDC} is higher than for $M>0$ and is localized between $z=8.0$ and $z=9.0$.

When we increase the absolute value of M, we do not observe the transient wavy-concentration profile as for $M>0$, but there is an additional deformation of the front that increases with $|M|$ (see Fig. 13 for $M=-1000$). However, this deformation does not disappear but corresponds to an asymptotic modulation in the asymptotic velocity and averaged concentration profiles, presented, respectively, in Figs. 14 and 15(a). The velocity profiles show that the convection roll here is constituted of a pronounced upward flow at the tip and a weaker downward flow at the back with larger

spatial extent. This is similar to the situation of positive M, except for the rotating direction determined by the sign of the surface tension gradient. This asymmetry along x as well as the width of the roll increase with $|M|$ but those effects are much less pronounced than for $M>0$. The asymptotic averaged and surface concentration profiles exhibit the same behavior but it is noticeable that only the back of these profiles is affected by the convection in a significant way (see Fig. 15). To end up with the characterization of the velocity profiles along x, let us notice that the global extrema of those profiles are more or less localized at the same distance from $\langle c\rangle=0.5$ for each $M<0$ which is different from the case of $M>0$. Figure 16 represents the asymptotic profiles of u across the layer, taken at the position along x where $|u|$ is maximum for various negative M. We can observe that the flow changes its direction and reaches its extremum values at the same heights for the different M and independently of their sign (cf. Fig. 10).

We have next made a comparison of the properties of the asymptotic dynamics for both positive and negative Marangoni numbers. Figure 17(a) shows that the asymptotic mixing length W of the front also increases with negative M but in a less pronounced way. The same observations apply to the propagation speed V of the nonlinear front and convection roll, but still indicating that the front always propagates faster in the presence of convection than by RD mechanisms, even if this effect is less pronounced for $M<0$ [see Fig. 17(b)]. On the contrary, when we plot the maximum absolute value of the asymptotic horizontal velocity u as a function of M [see Fig. 17(c)], we can observe that the convective motions are more important for $M<0$. In that case, the maximum value is also located at the surface where $u<0$ and is directed towards the products. Moreover, the
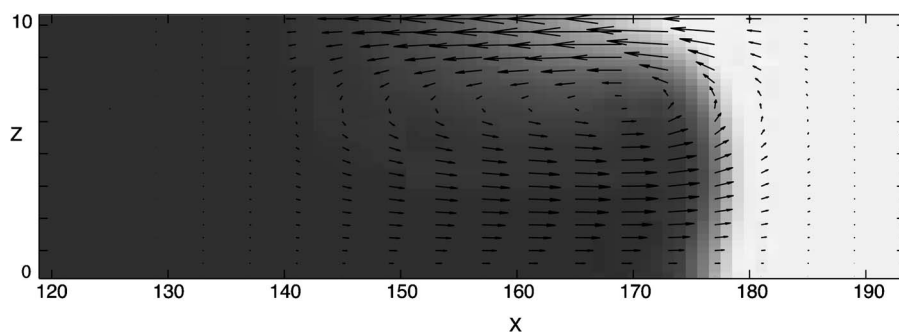

FIG. 12. Focus on the asymptotic asymmetric convection roll traveling with the deformed front for $M=-100$. The z direction is magnified compared with the x direction, cf. caption of Fig. 3.
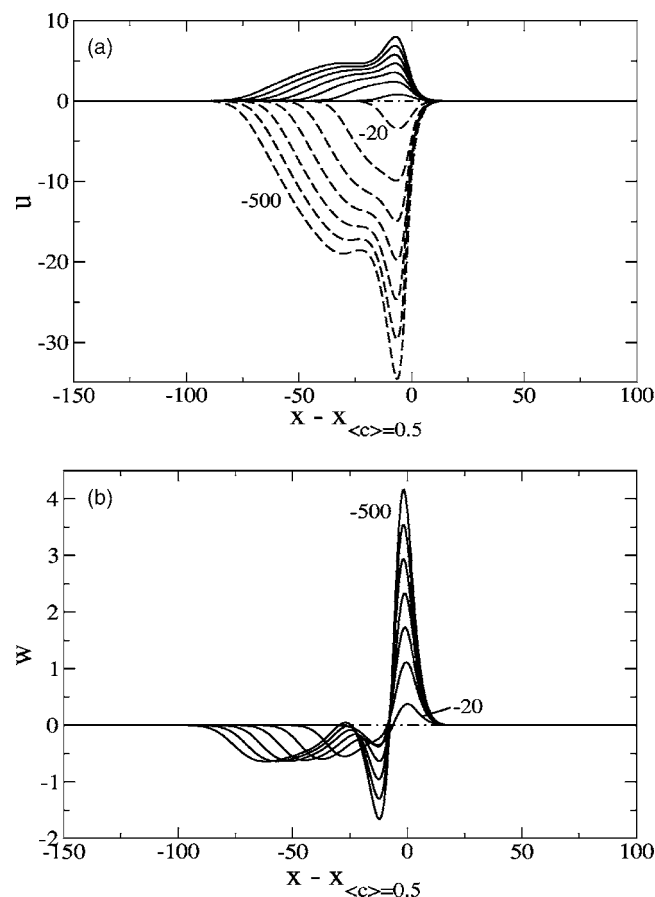
FIG. 14. Asymptotic profiles of (a) the horizontal velocity u at the surface (dashed lines) and in the middle of the layer (solid lines) and of (b) the vertical velocity w in the middle of the layer, represented in the comoving frame for decreasing negative Marangoni numbers between -20 and -500 with an interval of 80 between two successive curves. The dot-dashed curve corresponds to $M=0$ when there is no convection.
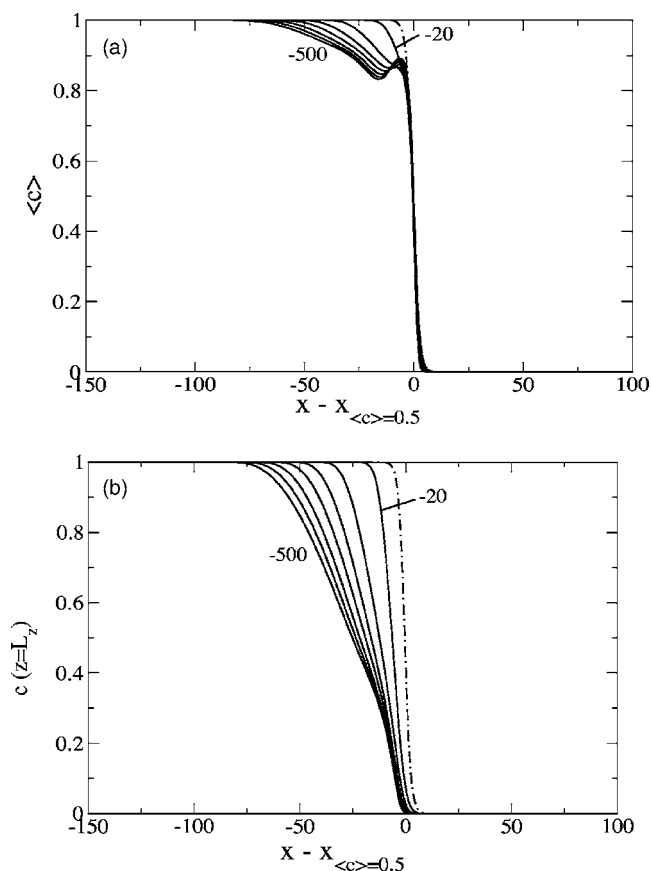

FIG. 15. Asymptotic profiles of (a) the averaged concentration $\langle c \rangle$ and of (b) the surface concentration, represented in the comoving frame for decreasing negative Marangoni numbers between -20 and -500 with an interval of 80 between two successive curves. The dot-dashed curve corresponds to the RD profile.

maximum value of u is not proportional to the square root of M but is a linear function of negative Marangoni numbers for $M \leqslant -60$.

C. Discussion

The different characteristics of the dynamics between $M > 0$ and $M < 0$ could be explained by the fact that the flow induced at the surface is then, respectively, parallel or antiparallel to the propagation direction of the front. Since convection is driven and sustained by forces at the surface, we expect these two situations to lead to different effects. First of all, let us recall that increasing the absolute value of M enhances the deformation of the front, leading to a weaker concentration gradient at the surface (larger w_{RDC} at $z=L_z$). However, as already observed by Dagan and Pismen in chemically induced Marangoni convection,[39] the intensity of the total surface force, given by $|M \partial c_s / \partial x|$, where $c_s = c(z=L_z)$, always increases with $|M|$. Furthermore, we have observed that the maximum absolute value of the horizontal fluid velocity u is proportional to the maximum value of $|M \partial c_s / \partial x|$. Since the propagation of the front for $M < 0$ opposes the direction of the flow, we expect the effects of the convection on the chemical front properties to be weaker than for $M > 0$. In particular, we expect a weaker deforma-

tion of the front (smaller w_{RDC} at $z=L_z$), leading to a larger surface force and hence to a larger maximum value of $|u|$. Indeed, we have measured that for the same absolute value of M, the driving force of convection is more important at $M < 0$, leading to the properties of Fig. 17(c). This could also possibly explain the reach of the stationary dynamics in terms of two opposed processes: the surface force, generated by the concentration gradient, enhances convection, which in
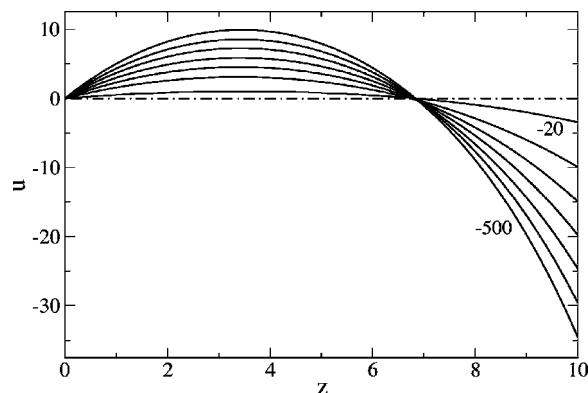

FIG. 16. Asymptotic profiles of the horizontal fluid velocity u across the layer at $x=x_{|u|=|u|_{max}}$ for decreasing negative Marangoni numbers between -20 and -500 with an interval of 80 between two successive curves. The dot-dashed curve corresponds to $M=0$ when there is no convection.
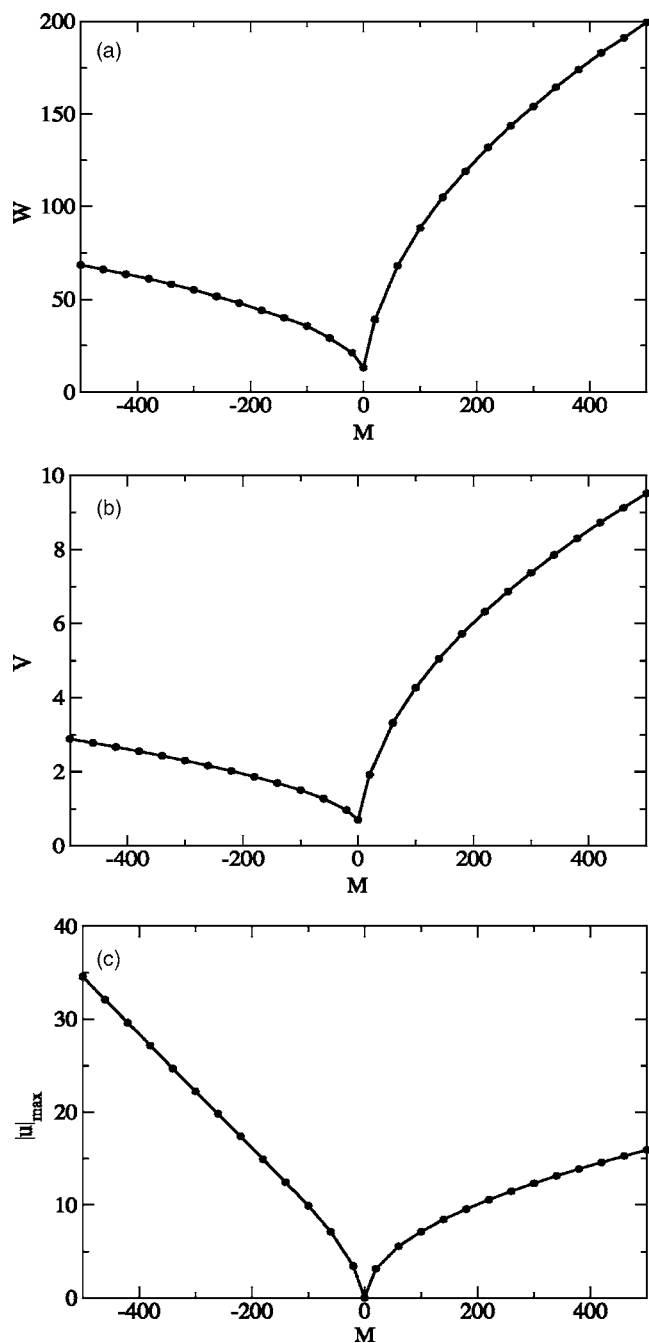
FIG. 17. (a) Asymptotic mixing length W, (b) propagation speed V, and (c) maximum absolute value of the asymptotic horizontal velocity u as a function of the Marangoni number.

that the position of zero velocity would be located around $z=2L_z/3$. The asymmetry along x can be explained by considering the asymptotic concentration profiles at the surface [Figs. 9(b) and 15(b)]. We have noticed that the position where the concentration gradient and hence the surface tension gradient are maximum is at the very tip of the front, where the concentration of the product is nearly zero. This leads to an asymmetric profile of the surface force, $|M\partial c_s/\partial x|$, and therefore to an asymmetry in the velocity profiles, independently of the sign of M (Figs. 8 and 14). However, the extrema of these profiles behave differently in the two situations. This may also find its origin in the surface concentration profiles. For positive M, the concentration profile extends further away from $\langle c\rangle=0.5$ when M increases, leading to a shift of the maximum concentration gradient, and consequently of the fluid velocity extrema. On the contrary, the end of the concentration profile is nearly unaffected by the variation of negative M, which explains that the extrema of the fluid velocity are localized at the same position in the comoving frame.

IV. CONCLUSIONS

We have numerically characterized the nonlinear dynamics resulting from the interaction of a chemical front with a pure solutal Marangoni effect induced by the concentration gradient at the surface of the solution layer. We find that when an autocatalytic chemical front propagates in the presence of chemically induced Marangoni convection, the system reaches an asymptotic dynamics characterized by a convection roll surrounding the reaction front and deforming it. In this asymptotic regime, the front propagates at a constant speed V, which is larger than the RD speed v and which increases with the Marangoni number M, measuring here the intensity of the coupling between RD processes and hydrodynamics. The reaction-diffusion-convection front is not planar anymore but deformed across the layer. However, its shape as well as the fluid velocity field are steady in a reference frame moving with velocity V. The steady traveling velocity field corresponds to an asymmetric convection roll localized in the region of the front.

We have shown that, for a similar intensity of the coupling, the stationary regime is reached sooner and the convective motions are more important when $M<0$ (product increasing the surface tension) than when $M>0$ (product decreasing the surface tension). However, the deformation of the front and its propagation speed are more important for $M>0$. This difference of behavior can mainly be explained by the fact that the flow induced at the surface is, respectively, parallel ($M>0$) or antiparallel ($M<0$) to the direction of front propagation.

This work calls for further extensions. First of all, it would be of interest to understand the nature of the transient oscillatory dynamics arising at large positive Marangoni numbers, when the product decreases the surface tension behind the front. For $M<0$, no transient oscillations are observed but a stationary additional deformation propagates with the front. The difference between these behaviors still remains to be investigated. After characterizing the interac-

turn spreads out the front and acts as to decrease the concentration gradient. For $M<0$, the more direct opposition between the chemical front propagation to the right and the surface fluid motion to the left can lead to an earlier reach of the stationary dynamics. However, different time scales between hydrodynamics and reaction-diffusion processes certainly play a role in these behaviors too and should be investigated in more detail to complete this hypothesis.

The fluid velocity field also exhibits differences following the sign of M, but the asymmetry along both the x and z directions is a common property. The height where the flow changes its direction is shifted towards the surface, and preliminary results with different layer thicknesses L_z indicate

tion of a chemical front with a pure solutal Marangoni instability, it would be interesting to see how this system couples to buoyancy-driven instabilities. In particular, the dependence of the asymptotic dynamics on the layer thickness should be investigated both for pure Marangoni effect and for the two coupled hydrodynamic instabilities. Indeed, the depth dependence of the dynamics has received much interest in various chemical systems.[7,8,15,16,24–26] Next, different effects may be progressively added to the model, such as the thermal effects linked to the enthalpy of the reaction[8,16] or to evaporative cooling arising in uncovered layers.[9]

ACKNOWLEDGMENTS

[1] *Oscillations and Traveling Waves in Chemical Systems*, edited by R. J. Field and M. Burger (Wiley, New York, 1985).
[2] I. R. Epstein and J. A. Pojman, *An Introduction to Nonlinear Chemical Dynamics* (Oxford University Press, Oxford, 1998).
[3] J. D. Murray, *Mathematical Biology* (Springer, Berlin, 2002).
[4] W. van Saarloos, Phys. Rep. **386**, 29 (2003).
[5] T. A. Gribschaw, K. Showalter, D. L. Banville, and I. R. Epstein, J. Phys. Chem. **85**, 2152 (1981).
[6] A. Hanna, A. Saul, and K. Showalter, J. Am. Chem. Soc. **104**, 3838 (1982).
[7] G. Bazsa and I. R. Epstein, J. Phys. Chem. **89**, 3050 (1985).
[8] J. A. Pojman and I. R. Epstein, J. Phys. Chem. **94**, 4966 (1990).
[9] J. C. Micheau, M. Gimenez, P. Borckmans, and G. Dewel, Nature (London) **305**, 43 (1983).
[10] D. Avnir and M. Kagan, Nature (London) **307**, 717 (1984).
[11] D. Avnir and M. Kagan, Chaos **5**, 589 (1995).
[12] M. Watzl and A. F. Münster, J. Phys. Chem. A **102**, 2540 (1998).
[13] A. J. Pons, F. Sagués, M. A. Bees, and P. G. Sorensen, J. Phys. Chem. B **104**, 2251 (2000).
[14] M. J. B. Hauser and R. H. Simoyi, Phys. Lett. A **191**, 31 (1994).
[15] B. S. Martincigh and R. H. Simoyi, Phys. Rev. E **52**, 1606 (1995).
[16] B. S. Martincigh and R. H. Simoyi, J. Phys. Chem. A **106**, 482 (2002).
[17] H. Miike, S. C. Müller, and B. Hess, Chem. Phys. Lett. **144**, 515 (1988).
[18] H. Miike, S. C. Müller, and B. Hess, Phys. Rev. Lett. **61**, 2109 (1988).
[19] K. Matthiessen and S. C. Müller, Phys. Rev. E **52**, 492 (1995).
[20] H. Miike and S. C. Müller, Chaos **3**, 21 (1993).
[21] T. Sakurai, E. Yokoyama, and H. Miike, Phys. Rev. E **56**, R2367 (1997).
[22] H. Miike, H. Yamamoto, S. Kai, and S. C. Müller, Phys. Rev. E **48**, R1627 (1993).
[23] S. Kai and H. Miike, Physica A **204**, 346 (1994).
[24] S. Kai, T. Ariyoshi, S. Inanaga, and H. Miike, Physica D **84**, 269 (1995).
[25] O. Inomoto, T. Ariyoshi, S. Inanaga, and S. Kai, J. Phys. Soc. Jpn. **64**, 3602 (1995).
[26] O. Inomoto, S. Kai, T. Ariyoshi, and S. Inanaga, Int. J. Bifurcation Chaos Appl. Sci. Eng. **7**, 989 (1997).
[27] H. Kitahata, R. Aihara, N. Magome, and K. Yoshikawa, J. Chem. Phys. **116**, 5666 (2002).
[28] H. Kitahata and K. Yoshikawa, Physica D **205**, 283 (2005).
[29] K. Yoshikawa, T. Kusumi, M. Ukitsu, and S. Nakata, Chem. Phys. Lett. **211**, 211 (1993).
[30] O. Inomoto, K. Abe, T. Amemiya, T. Yamaguchi, and S. Kai, Phys. Rev. E **61**, 5326 (2000).
[31] T. Plesser, H. Wilke, and K. H. Winters, Chem. Phys. Lett. **200**, 158 (1992).
[32] D. A. Vasquez, J. M. Littley, J. W. Wilder, and B. F. Edwards, Phys. Rev. E **50**, 280 (1994).
[33] H. Wilke, Physica D **86**, 508 (1995).
[34] Y. Wu, D. A. Vasquez, B. F. Edwards, and J. W. Wilder, Phys. Rev. E **51**, 1119 (1995).
[35] K. A. Cliffe, S. J. Tavener, and H. Wilke, Phys. Fluids **10**, 730 (1998).
[36] V. Pérez-Villar, A. P. Muñuzuri, and V. Pérez-Muñuzuri, Phys. Rev. E **61**, 3771 (2000).
[37] K. Matthiessen, H. Wilke, and S. C. Müller, Phys. Rev. E **53**, 6056 (1996).
[38] M. Diewald, K. Matthiessen, S. C. Müller, and H. R. Brand, Phys. Rev. Lett. **77**, 4466 (1996).
[39] Z. Dagan and L. M. Pismen, J. Colloid Interface Sci. **99**, 215 (1984).
[40] Z. Dagan and C. Maldarelli, Chem. Eng. Sci. **42**, 1259 (1987).
[41] L. M. Pismen, J. Colloid Interface Sci. **102**, 237 (1984).
[42] L. M. Pismen, Phys. Rev. Lett. **78**, 382 (1997).
[43] K. Showalter, in *Kinetics of Nonhomogenous Processes*, edited by G. R. Freeman (Wiley, New York, 1987), p. 769.
[44] A. A. Nepomnyashchy, M. G. Velarde, and P. Colinet, *Interfacial Phenomena and Convection* (Chapman and Hall, London/CRC, Boca Raton, 2002).
[45] H. Malchow and L. Shimansky-Geier, *Noise and Diffusion in Bistable Nonequilibrium Systems* (Teubner, Leipzig, 1985).
[46] W. T. Vetterling, S. A. Teukolsky, W. H. Press, and B. P. Flannery, *Numerical Recipes in C* (Cambridge University Press, Cambridge, 1992).
[47] P. M. Gresho and R. L. Sani, Int. J. Numer. Methods Fluids **7**, 1111 (1987).